Rapid Communications | Editors' Suggestion

Mimicking chiral light-matter interaction

Sergey Nechayev* and Peter Banzer
Max Planck Institute for the Science of Light, Staudtstr. 2, D-91058 Erlangen, Germany
and Institute of Optics, Information and Photonics, University Erlangen-Nuremberg, Staudtstr. 7/B2, D-91058 Erlangen, Germany

(Received 3 April 2019; revised manuscript received 23 May 2019; published 4 June 2019)

We demonstrate that achiral electric-dipole scatterers can mimic an interaction of light with chiral matter by generating far-field circular polarization upon scattering, even though the optical chirality of the incident field as well as that of the scattered light is zero. On the one hand, the presented effect originates from the fact that electric-dipole scatterers respond selectively only to the incident electric field, which eventually results in depolarization of the transmitted beam and in generation of far-field circular polarization. On the other hand, although the incident beam does not possess any optical chirality, it lacks reflection symmetry and therefore it is geometrically chiral. To experimentally demonstrate this effect, we utilize a cylindrical vector beam with spiral polarization and a spherical gold nanoparticle positioned on the optical axis—the axis of rotational symmetry of the system. Our experiment and a simple theoretical model address the fundamentals of duality symmetry in optics and chiral light-matter interactions, accentuating their richness and ubiquity yet in highly symmetric configurations.

DOI: 10.1103/PhysRevB.99.241101

I. INTRODUCTION

Chiral light-matter interactions attract tremendous attention in modern classical [1–5] and quantum optics [6–9]. Describing chiral light-matter interactions requires characterization of optical chirality of the incoming and outgoing electromagnetic field [10]. For quasimonochromatic fields with a time-harmonic dependence, which are the subject of the current paper, optical chirality [10] is closely related to helicity [11–16]—a quantity that measures whether the total angular momentum is aligned or antialigned with linear momentum [12,17,18]. The helicity density of a quasimonochromatic electromagnetic field $K \propto \Im(\mathbf{E}^* \cdot \mathbf{H})$ in the far field is proportional to the degree of circular polarization of each individual plane wave, expressed via the angularly resolved third Stokes parameter $S_3(\mathbf{k})$, where $\mathbf{k}$ is the wave vector. In focused fields, K is proportional to a difference between the integrated contributions of all right- and left-hand circularly polarized (RCP and LCP) plane waves to the focal field [11,12,14–20]. Owing to the fundamental relation between optical chirality and helicity density K for quasimonochromatic electromagnetic fields, extinction of helicity from an incident field in the course of light-matter interaction is usually a clear signature of interaction of matter and light chirality [15–23]. Selective extinction or generation of helicity by chiral molecules upon interaction with the incident light was first observed by Haidinger in 1847, and it was termed *circular dichroism* by Cotton in 1895 and became the most important tool in identifying chiral objects since then [24].

Here, we present a counterintuitive case of interaction between an electric-dipole scatterer and a vector beam that doesn't possess any optical chirality [10] in cylindrically symmetric configuration. The interaction results in generation of circular polarization, effectively mimicking an interaction of light with chiral matter [21–24]. Specifically, we show that scattering of a focused cylindrical vector beam with spiral polarization [25,26] by an electric-dipole scatterer generates far-field helicity. Notwithstanding that the incident beam, the focal fields, as well as the scattered light bear zero optical chirality and the scatterer is positioned on the optical axis—the axis of rotational symmetry of the system. Moreover, the whole experimental system is cylindrically symmetric and independent of the direction of incidence of the beam [27–29]. The physical origin of the effect is related to two facts. First, electric-dipole scatterers break the electromagnetic duality symmetry [12,14,15,17,18,30–32] by responding selectively only to the incident electric field components. Second, although our vector beam does not possess any optical chirality [10], it lacks reflection symmetry. Based on this, the experiment can be explained in terms of the superposition of the transverse electric (TE or azimuthal) component of the incident beam and the phase-delayed transverse magnetic (TM or radial) component of the scattered light. Our experiment and a simple theoretical model shed light on chiral light-matter interactions and helicity conservation laws in electromagnetism.

II. THEORY

For the theoretical treatment, we consider a system consisting of two confocally aligned aplanatic microscope objectives (MOs) with focal lengths f and numerical apertures $\mathrm{NA} = \mathrm{NA}_1 = \mathrm{NA}_2$ with the surrounding refractive index $n = n_1 = n_2 = 1$, as shown in Fig. 1(a). The incident spirally polarized cylindrical vector beam (SPCVB) [25], schematically shown in Fig. 1(b), propagating along the z axis is focused by the first MO, while the second MO collects and collimates the transmitted light. The incident field distributions in the back

*sergey.nechayev@mpl.mpg.de

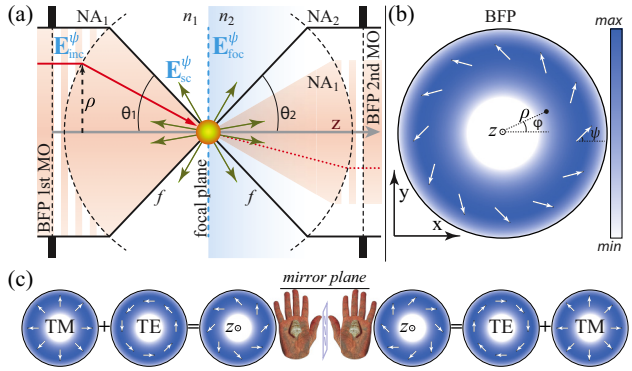

FIG. 1. (a) An aplanatic high numerical aperture (NA) microscope objective (MO) focuses the incident field distribution in its back focal plane (BFP) $\mathbf{E}^{\psi}_{\text{inc}}$. The focal plane ($z = 0$) constitutes a boundary between two dielectric media with refractive indices n_1 and n_2. The focal field $\mathbf{E}^{\psi}_{\text{foc}}$ excites a spherical electric-dipole-like nanoparticle positioned along the optical axis z at the position $z = z_0$. The second confocally aligned index-matched aplanatic MO collimates the incident beam and collects the scattered light $\mathbf{E}^{\psi}_{\text{sc}}$. The interference pattern of $\mathbf{E}^{\psi}_{\text{inc}}$ and $\mathbf{E}^{\psi}_{\text{sc}}$ is observed in the BFP of the second MO. The theoretical description is given for the case of $n_1 = n_2 = 1$, $\text{NA}_1 = \text{NA}_2 = 1$, and $z_0 = 0$. In the experimental section, we use $n_1 = 1$, $n_2 = 1.52$, $\text{NA}_1 = n_1 \max\{\sin(\theta_1)\} = 0.9$, $\text{NA}_2 = n_2 \max\{\sin(\theta_2)\} = 1.3$, and $z_0 = -d/2 = 70\,\text{nm}$, where $d = 140\,\text{nm}$ is the diameter of the nanoparticle. (b) Distribution of the incident spirally polarized cylindrical vector beam (SPCVB) in the BFP of the first MO. The intensity pattern is shown as the color map, while the white arrows depict the polarization pattern. (c) Mirror reflection properties of a SPCVB with $\psi = +45^\circ$, which can be represented as an in-phase superposition of a radially (TM) and azimuthally (TE) polarized beams with equal amplitudes. The TE component acquires a π phase upon mirror reflection, which switches the sense of rotation of the SPCVB and the angle to $\psi = -45^\circ$. Importantly, this SPCVB is a three-dimensional chiral object, similar to a seashell or a human hand, while the third dimension corresponds to the propagation direction or the optical axis z.

focal planes (BFP) of both MOs are given by

$$\mathbf{E}^{\psi}_{\text{inc}} \equiv E_{\text{in}}\mathbf{e}_{\text{in}} = E_{\text{in}}(\cos(\psi)\hat{\boldsymbol{\rho}} + \sin(\psi)\hat{\boldsymbol{\varphi}}),$$
$$\mathbf{H}^{\psi}_{\text{inc}} \equiv \frac{E_{\text{in}}}{\eta}\mathbf{h}_{\text{in}} = \frac{E_{\text{in}}}{\eta}(\cos(\psi)\hat{\boldsymbol{\varphi}} - \sin(\psi)\hat{\boldsymbol{\rho}}), \qquad (1)$$

with a doughnut-shaped amplitude profile $E_{\text{in}} = E_0\frac{\rho}{w_0}\exp(-\frac{\rho^2}{w_0^2})$, where w_0 is the beam waist, η is the free-space impedance, ρ and φ are the radial and axial cylindrical coordinates, respectively, $\hat{\boldsymbol{\rho}}$ and $\hat{\boldsymbol{\varphi}}$ are the corresponding cylindrical unit vectors, ψ defines the spiral polarization angle, and $E_0 = 1$ without the loss of generality. Aplanatic MOs link the field distributions in their BFPs to the far field or the k-space of the focused beam via $\boldsymbol{\rho} = -\frac{f}{k_0}(k_x, k_y)$ [33]. In the following, we refer to the BFP coordinates as *angularly resolved*. The beam in Eq. (1), schematically shown in Fig. 1(b), is cylindrically symmetric with respect to the optical axis z and it is linearly polarized in each point of the BFPs. Consequently, it has zero helicity density $K^{\psi}_{\text{in}} = 0$ everywhere in the beam cross section. Nevertheless, a peculiarity of these vector beams is that they possess a geometric sense of chirality for $\psi \neq m \times 90^\circ$, where m is an integer number, which can be shown by considering their properties upon reflection in a mirror plane that contains the optical axis z. The left-hand side of Fig. 1(c) shows a SPCVB with $\psi = +45^\circ$, which can be presented as an in-phase superposition of radially (TM) and azimuthally (TE) polarized beams with equal amplitudes. Upon mirror reflection, as shown in the right-hand side of Fig. 1(c), the TE component acquires a phase of π, resulting in the change of the sense of rotation of the SPCVB and a change of its angle to $\psi = -45^\circ$. Importantly, the beam in Fig. 1(c) is a three-dimensional (3D) chiral object [21–24], while the third dimension corresponds to the propagation direction—the optical axis z. Therefore, a mirror reflection changes the 3D handedness of the SPCVB, similar to the reflection of a seashell or a human hand, emphasizing the geometrical chirality of such beams [34].

The fields in the proximity of the optical axis in the focal plane ($\rho \approx 0$, $z = 0$) produced by the first MO are given by [33,35,36]

$$\mathbf{E}^{\psi}_{\text{foc}}(\mathbf{r}) = A\left(\cos(\psi)\left\{\rho\hat{\boldsymbol{\rho}} + \frac{2\imath}{k_{\text{eff}}}\hat{\mathbf{z}}\right\} + \sin(\psi)\frac{k_0}{k_{\text{eff}}}\rho\hat{\boldsymbol{\varphi}}\right),$$
$$\mathbf{H}^{\psi}_{\text{foc}}(\mathbf{r}) = B\left(\cos(\psi)\frac{k_0}{k_{\text{eff}}}\rho\hat{\boldsymbol{\varphi}} - \sin(\psi)\left\{\rho\hat{\boldsymbol{\rho}} + \frac{2\imath}{k_{\text{eff}}}\hat{\mathbf{z}}\right\}\right), \qquad (2)$$

where k_{eff} is the effective wave number and A, $B \in \mathbb{R}$, $B = A\eta^{-1}$ are the proportionality constants [37]. For symmetry reasons, the fields along the optical axis ($\rho = 0$) have strictly zero helicity density $K^{\psi}_{\text{foc}} = 0$ also for the case of $n_1 \neq n_2$ that includes reflection [33]. We assume that the fields in Eqs. (2) excite an electric-dipole-like spherical gold nanoparticle positioned in the focus $\mathbf{r}_0 = \mathbf{r}(\rho, z = 0)$. We also assume that this scatterer responds only to the local electric field and the induced electric dipole moment is $\mathbf{p} = \alpha_e\varepsilon_0\mathbf{E}^{\psi}_{\text{foc}}(\mathbf{r}_0) \equiv (0, 0, p_z)$, where α_e is the electric-dipole polarizability, $k_0 = 2\pi/\lambda$ is the free-space wave number, λ is the free-space wavelength, and ε_0 is the vacuum permittivity. Importantly, in free space, the electric-dipole polarizability α_e of a spherical nanoparticle is in quadrature ($\pi/2$ phase delayed) with its first Mie coefficient a_1 and is given by $\alpha_e = (6\pi\imath/k_0^3)a_1$ [38]. For a dipole moment oriented along the optical axis, the scattered light $\mathbf{E}^{\psi}_{\text{sc}}$ collected by the second MO is purely radially polarized [33,39,40],

$$\mathbf{E}^{\psi}_{\text{sc}} = -CD\frac{\rho}{f}p_z\hat{\boldsymbol{\rho}} = GDa_1\cos(\psi)\frac{\rho}{f}\hat{\boldsymbol{\rho}},$$
$$\mathbf{H}^{\psi}_{\text{sc}} = -CD\frac{\rho}{f\eta}p_z\hat{\boldsymbol{\varphi}} = GDa_1\cos(\psi)\frac{\rho}{f\eta}\hat{\boldsymbol{\varphi}}, \qquad (3)$$

where $C = \frac{k_0^2}{4\pi\varepsilon_0 f}$, $D = [1 - (\rho/f)^2]^{-1/4}$, and $G = \frac{3A}{k_0 f k_{\text{eff}}}$. Here, the scattered field also has strictly zero helicity density $K^{\psi}_{\text{sc}} \propto \Im(\mathbf{E}^{\psi\,*}_{\text{sc}} \cdot \mathbf{H}^{\psi}_{\text{sc}}) = 0$. Surprisingly, the total field $\mathbf{E}^{\psi}_{\text{tot}} = \mathbf{E}^{\psi}_{\text{inc}} + \mathbf{E}^{\psi}_{\text{sc}}$ in the BFP of the collecting MO acquires a nonzero helicity density K^{ψ}_{tot}, which can be expressed as the angularly resolved third Stokes parameter $S_3(\rho)$:

$$\begin{aligned} S_3(\rho) &= 2\Im\left\{\left(\mathbf{E}^{\psi}_{\text{tot}}\cdot\hat{\boldsymbol{\rho}}\right)^*\left(\mathbf{E}^{\psi}_{\text{tot}}\cdot\hat{\boldsymbol{\varphi}}\right)\right\} \\ &= 2\Im\left\{\left(\mathbf{E}^{\psi}_{\text{sc}}\cdot\hat{\boldsymbol{\rho}}\right)^*\left(\mathbf{E}^{\psi}_{\text{inc}}\cdot\hat{\boldsymbol{\varphi}}\right)\right\} \\ &= -\sin(2\psi)\Im\{a_1\}GD\frac{\rho}{f}E_{\text{in}}. \end{aligned} \qquad (4)$$

Equation (4) highlights the main theoretical result of this paper. First, the far-field helicity is generated owing to the superposition between the azimuthally polarized component of the incident beam and the phase-delayed radially polarized component of the scattered light. Particularly, it is the nonzero phase of a_1 that delays the scattered light with respect to the incident beam and results in $S_3(\rho) \neq 0$, as appears in Eqs. (3) and (4). Moreover, in our case, the generation of far-field helicity is an off-resonance effect [16,20,41]—$S_3(\rho)$ in Eq. (4) is proportional to $\Im(a_1)$ or $\Re(\alpha_e)$, contrary to the resonant effect of extinction of energy, which is proportional to $\Re(a_1)$ or $\Im(\alpha_e)$ [16,20,38]. Second, it is remarkable that helicity is extinguished by an achiral electric-dipole scatterer positioned at a point where the helicity density of the excitation field $K^{\psi}_{\rm foc}$ is zero, in sharp contrast to the mechanism of energy extinction that requires nonzero energy density [16]. Lastly, the scattered helicity $\propto \Im(\mathbf{p}\cdot\mathbf{m}^*)$ [15,42] is also zero, since there is no excited magnetic dipole moment $\mathbf{m} = 0$ for an ideal electric-dipole scatterer. Here, we emphasize that since the scattered helicity, the incident helicity, and the incident helicity density are zero, the extinction of helicity from the incident beam given by Eq. (4) originates from helicity *conversion* or *creation* [41] (for discussion, see Ref. [43]). In this case, the extinction of helicity from the incoming beam $\mathcal{W}_{\mathcal{H}}$ can be calculated as a projection of the induced electric dipole moment on the magnetic focal field $\mathcal{W}_{\mathcal{H}} \propto -\Re\{\mathbf{p}\cdot\mathbf{H}^{\psi *}_{\rm foc}(\mathbf{r}_0)\}$ [15]. On the one hand, substituting the expression for the dipole moment $\mathbf{p}$, we get $\mathcal{W}_{\mathcal{H}} \propto \Im\{a_1\mathbf{E}^{\psi}_{\rm foc}(\mathbf{r}_0)\cdot\mathbf{H}^{\psi *}_{\rm foc}(\mathbf{r}_0)\}$, which resembles the definition of the helicity density of the focal fields $K^{\psi}_{\rm foc}$ modified by the Mie coefficient a_1. On the other hand, substituting the fields in Eqs. (2), we get $\mathcal{W}_{\mathcal{H}} \propto -\sin(2\psi)\Im(a_1)$, showing near-field to far-field [Eq. (4)] correspondence.

III. EXPERIMENT

Our experimental setup, described in detail in our previous works [26,44], is shown as a simplified sketch in Fig. 2(a). We convert an incoming linearly polarized Gaussian beam into a SPCVB using a q-plate [45] of charge 1/2. We spatially filter the SPCVB [46] and focus it by the first MO with $\mathrm{NA}_1 = 0.9$. A gold [47] nanosphere of diameter $d = 140\,\mathrm{nm}$ is positioned on the optical axis z in air ($n_1 = 1$) above a glass substrate ($n_2 = 1.52$) at $z = -d/2 = -70\,\mathrm{nm}$. Mie theory [38] predicts that such a nanoparticle in free space behaves dominantly as an electric-dipole scatterer in the wavelength range $520\,\mathrm{nm} \leqslant \lambda \leqslant 700\,\mathrm{nm}$. The glass substrate is mounted onto a 3D piezo actuator, allowing for precise positioning of the nanoparticle in the focal volume. The transmitted and scattered light are collected by the second confocally aligned index-matched immersion-type MO ($\mathrm{NA}_2 = 1.3$), while the focal plane ($z = 0$) of both MOs constituting a boundary between two media. In our experimental scheme of the nanoparticle on a glass substrate with $\mathrm{NA}_2 > \mathrm{NA}_1$, the far-field interference of the incident and scattered light is obtained in the BFP of the second MO in the angular range $|n_2\sin(\theta_2)| \leqslant \max\{\sin(\theta_1)\} = \mathrm{NA}_1$, as schematically depicted in Fig. 1(a), while for $|n_2\sin(\theta_2)| > \max\{\sin(\theta_1)\} = \mathrm{NA}_1$ we collect only the scattered light, which allows us to experimentally verify

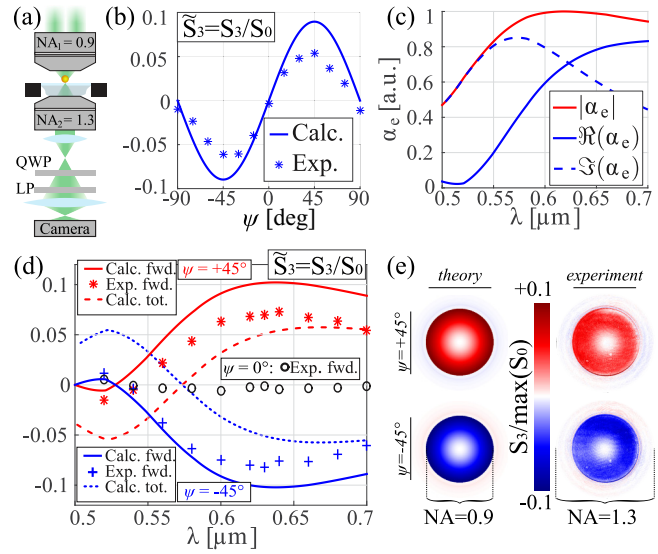

FIG. 2. (a) Sketch of the experimental setup. The incident beam is focused onto a gold nanoparticle by a microscope objective (MO). The light propagating in the forward direction is collected and collimated by an immersion-type MO and transmitted through an achromatic quarter-wave plate (QWP) and a rotatable linear polarizer (LP). A subsequent lens images the back focal plane of the second MO onto a camera. (b) The calculated (solid line) and measured (markers) averaged normalized value of the third Stokes parameter $\widetilde{S}_3$ as a function of the spiral polarization angle ψ at the wavelength of $\lambda = 600\,\mathrm{nm}$. (c) Longitudinal (along the substrate normal) electric-dipole polarizability α_e, normalized to its own maximal value, of a spherical gold particle of diameter $d = 140\,\mathrm{nm}$ positioned on a glass substrate with the refractive index $n = 1.52$. (d) The calculated (solid lines) and measured (markers) $\widetilde{S}_3$ in the forward scattering hemisphere (fwd.) as a function of wavelength for the spiral polarization angles $\psi = +45^\circ$ (red) and $\psi = -45^\circ$ (blue). The red dashed and blue dotted lines display the corresponding calculated $\widetilde{S}_3$ over the full 4π solid angle (tot.), showing the overall degree of polarization handedness. The black circles show the measured $\widetilde{S}_3$ for radial excitation $\psi = 0^\circ$. (e) Calculated (left column) and measured (right column) angularly resolved S_3 parameters for $\psi = +45^\circ$ (top row) and $\psi = -45^\circ$ (bottom row) at $\lambda = 630\,\mathrm{nm}$, normalized to the maximal value of S_0. These images show that S_3 is only significant in the angular region containing both the incident and the scattered light ($\mathrm{NA} \leqslant 0.9$), while the scattered light itself ($0.9 < \mathrm{NA} \leqslant 1.3$) does not contain significant circular polarization.

independently our theoretical predictions in Eqs. (3) and (4). We image the BFP of the second MO onto an achromatic quarter-wave plate and a linear polarizer to project the field distribution in the BFP onto RCP or LCP. The second lens in Fig. 2(a) images the projected BFP intensity distribution $I_{\rm RCP}$ or $I_{\rm LCP}$ onto a camera, which allows us to measure the far-field angularly resolved Stokes parameters $S_0(\mathbf{k}) = I_{\rm LCP} + I_{\rm RCP}$ and $S_3(\mathbf{k}) = I_{\rm LCP} - I_{\rm RCP}$. We background-correct each measurement by transmitting the excitation beam through the substrate only. To obtain the overall values of S_0 and S_3, we integrate $S_0(\mathbf{k})$ and $S_3(\mathbf{k})$ across the BFP.

To theoretically describe the practical experimental conditions, we include in our theory the actual incident beam and apertures' sizes, the position of the scatterer on the optical axis, the contribution of reflection to the focal fields,

dressed electric-dipole and magnetic-dipole polarizabilities of the scatterer [48,49], Fresnel coefficients, and energy conservation factors [33].

First, we perform a measurement at $\lambda = 600\,\mathrm{nm}$ to verify the dependence of the generated far-field helicity on the incident spiral polarization angle ψ. In Fig. 2(b), we plot the normalized average value of the third Stokes parameter $\widetilde{S}_3 \equiv S_3/S_0$ along with its theoretical value for $-90^\circ \leqslant \psi \leqslant +90^\circ$. For incident radially (TM) ($\psi = 0^\circ$) and azimuthally (TE) polarized beams ($\psi = \pm 90^\circ$), only electric p_z and (a very small, but not strictly zero) magnetic m_z dipoles are symmetry allowed to be excited [39], featuring TM and TE polarized scattered light, respectively, resulting in $\widetilde{S}_3 = 0$. For $\psi = +45^\circ$ and $\psi = -45^\circ$, the far-field light is left- and right-handed elliptically polarized, respectively. The experimental results correctly resolve the dependence $\widetilde{S}_3 \propto \sin(2\psi)$, as predicted by Eq. (4).

Next, we study the spectrum of $\widetilde{S}_3 = S_3/S_0$ at the angles $\psi = \pm 45^\circ$. On the one hand, from Eq. (4), we expect the spectrum of S_3 to follow $\Im(a_1)$ [16,41] or, in our experimental configuration, the real part of the longitudinal (along the z axis) electric-dipole polarizability $\Re(\alpha_e)$ [48,49], which is plotted in Fig. 2(c). On the other hand, S_0 is inversely proportional to the extinction of light by the nanoparticle $\propto \Im(\alpha_e)$. As a result, both $\Re(\alpha_e)$ and $\Im(\alpha_e)$ influence the spectrum of $\widetilde{S}_3 = S_3/S_0$. In Fig. 2(d), we plot the resulting calculated and the experimentally obtained values of $\widetilde{S}_3$ for $\psi = +45^\circ$ and $\psi = -45^\circ$ in red and blue colors, respectively. Figure 2(d) confirms the generation of nonzero far-field helicity with the sign of $\widetilde{S}_3$ being dependent on ψ, in agreement with our theoretical model. For completeness, we also calculate the corresponding $\widetilde{S}_3$ over the full 4π solid angle, showing the overall degree of polarization handedness, plotted with the red dashed and blue dotted lines in Fig. 2(d). Additionally, we perform a calibration experiment with radially polarized excitation ($\psi = 0^\circ$), where the expected value of $\widetilde{S}_3$ is zero, shown as black circles in Fig. 2(c).

Lastly, we experimentally confirm that in the angular region $|n_2 \sin(\theta_2)| > \max\{\sin(\theta_1)\} = \mathrm{NA}_1$, where the scattered light does not interfere with the incident beam, the third Stokes parameter S_3 of the far-field light is close to zero. In Fig. 2(e), we plot the theoretically calculated (left column) and experimentally recorded (right column) angularly resolved S_3 parameters for $\psi = +45^\circ$ (top row) and $\psi = -45^\circ$ (bottom row) at $\lambda = 630\,\mathrm{nm}$, normalized to the maximum value of S_0. Figure 2(e) confirms that only within the angular range corresponding to the interference of the incident and scattered light ($\mathrm{NA} \leqslant 0.9$), we observe a significant value of S_3. On the contrary, in the angular range $0.9 \leqslant \mathrm{NA} \leqslant 1.3$, corresponding to the scattered light only, we obtain negligible values of $S_3 \approx 0$. The small (but nonzero) residual values in the angular range $0.9 \leqslant \mathrm{NA} \leqslant 1.3$ originate from the contribution of a small (but not strictly zero) magnetic dipole moment [26] supported by the gold nanoparticle.

IV. DISCUSSION

The observed effect can be understood by considering the helicity conservation laws, symmetry, and the duality properties of our system [12–15,17,18,22,23,30–32]. First, although our vector beam does not possess any optical chirality [10], it lacks mirror symmetry and therefore exhibits a geometric sense of chirality [21,24]. Second, electric-dipole scatterers break the electromagnetic duality symmetry by reacting selectively to electric field only. Systems that break the electromagnetic duality symmetry do not conserve helicity, i.e., they may change the average far-field degree of circular polarization [18], which we have experimentally confirmed. In the context of the helicity optical theorem [15,16,20], we have provided the first experimental proof of a pure conversion of helicity [41,43]. Specifically, there is extinction of helicity due to scattering by an electric dipole, but there is neither incident nor scattered helicity. This effect mimics an interaction of light with chiral matter [21–24]. Additionally, our system is also rotationally invariant, meaning that the total angular momentum of light J_z must be conserved. As a result, the emerging spin angular momentum in the region of $\mathrm{NA} \leqslant 0.9$ must be compensated by the generation of orbital angular momentum [50], i.e., the circularly polarized components of the beam shown in Fig. 2(e) have a helical phase distribution as a direct consequence of the phase-shifted superposition of azimuthal polarization of the excitation beam and radial polarization emitted by the nanoparticle [26]. Finally, the presented effect is determined by the longitudinal field components, accentuating their importance in the description of light-matter interaction [16,51–58].

V. CONCLUSION

In conclusion, we have theoretically and experimentally shown that scattering of a focused cylindrical vector beam with spiral polarization by an electric-dipole scatterer positioned on the optical axis generates far-field circular polarization. Notwithstanding that the incident beam, the focal fields, as well as the scattered light have zero optical chirality. The effect originates from the electromagnetic duality symmetry breaking by the scatterer, which selectively responds to the electric field only and from the geometric sense of chirality of the incident beam, manifested by the lack of reflection symmetry. It can be conveniently explained in terms of the superposition of the TE (azimuthal) component of the incident beam and the phase-delayed TM (radial) component of the scattered light. Utilizing a substrate supporting the scatterer allowed us to separate the angular region where the transmitted far-field interferes with the scattered light from the angular region that contains the scattered light only, facilitating experimental observation of our theoretical predictions. Our experiment and the simple theoretical model shed light on chiral light-matter interactions, helicity conservation laws in electromagnetism, and emphasize the role of duality symmetry in optics.

ACKNOWLEDGMENTS

We gratefully acknowledge fruitful discussions with Paweł Woźniak, Martin Neugebauer, Jörg S. Eismann, and Gerd Leuchs. The authors thank Eduard Butzen for providing the scanning electron microscopy images of the sample.

[1] V. I. Kopp, V. M. Churikov, J. Singer, N. Chao, D. Neugroschl, and A. Z. Genack, Science **305**, 74 (2004).

[2] K. Y. Bliokh, A. Niv, V. Kleiner, and E. Hasman, Nat. Photonics **2**, 748 (2008).

[3] W.-J. Chen, Z. H. Hang, J.-W. Dong, X. Xiao, H.-Z. Wang, and C. T. Chan, Phys. Rev. Lett. **107**, 023901 (2011).

[4] V. K. Valev, J. J. Baumberg, C. Sibilia, and T. Verbiest, Adv. Mater. **25**, 2517 (2013).

[5] R. P. Cameron, J. B. Götte, S. M. Barnett, and A. M. Yao, Philos. Trans. R. Soc. London A **375**, 20150433 (2017).

[6] Y. J. Zhang, T. Oka, R. Suzuki, J. T. Ye, and Y. Iwasa, Science **344**, 725 (2014).

[7] H. Pichler, T. Ramos, A. J. Daley, and P. Zoller, Phys. Rev. A **91**, 042116 (2015).

[8] C. Sayrin, C. Junge, R. Mitsch, B. Albrecht, D. O'Shea, P. Schneeweiss, J. Volz, and A. Rauschenbeutel, Phys. Rev. X **5**, 041036 (2015).

[9] P. Lodahl, S. Mahmoodian, S. Stobbe, A. Rauschenbeutel, P. Schneeweiss, J. Volz, H. Pichler, and P. Zoller, Nature **541**, 473 (2017).

[10] Y. Tang and A. E. Cohen, Phys. Rev. Lett. **104**, 163901 (2010).

[11] K. Y. Bliokh and F. Nori, Phys. Rev. A **83**, 021803(R) (2011).

[12] R. P. Cameron, S. M. Barnett, and A. M. Yao, New J. Phys. **14**, 053050 (2012).

[13] S. M. Barnett, R. P. Cameron, and A. M. Yao, Phys. Rev. A **86**, 013845 (2012).

[14] K. Y. Bliokh, A. Y. Bekshaev, and F. Nori, New J. Phys. **15**, 033026 (2013).

[15] M. Nieto-Vesperinas, Phys. Rev. A **92**, 023813 (2015).

[16] M. Nieto-Vesperinas, J. Opt. **19**, 065402 (2017).

[17] I. Fernandez-Corbaton, X. Zambrana-Puyalto, and G. Molina-Terriza, Phys. Rev. A **86**, 042103 (2012).

[18] I. Fernandez-Corbaton, X. Zambrana-Puyalto, N. Tischler, X. Vidal, M. L. Juan, and G. Molina-Terriza, Phys. Rev. Lett. **111**, 060401 (2013).

[19] K. Y. Bliokh, Y. S. Kivshar, and F. Nori, Phys. Rev. Lett. **113**, 033601 (2014).

[20] M. Nieto-Vesperinas, Philos. Trans. R. Soc. London A **375**, 20160314 (2017).

[21] I. Fernandez-Corbaton, M. Fruhnert, and C. Rockstuhl, Phys. Rev. X **6**, 031013 (2016).

[22] D. S. Bradshaw, J. M. Leeder, M. M. Coles, and D. L. Andrews, Chem. Phys. Lett. **626**, 106 (2015).

[23] F. Crimin, N. Mackinnon, J. B. Götte, and S. M. Barnett, Appl. Sci. **9**, 828 (2019).

[24] L. D. Barron, *Molecular Light Scattering and Optical Activity*, 2nd ed. (Cambridge University Press, Cambridge, UK, 2004).

[25] Q. Zhan and J. R. Leger, Opt. Express **10**, 324 (2002).

[26] J. S. Eismann, M. Neugebauer, and P. Banzer, Optica **5**, 954 (2018).

[27] X. Zambrana-Puyalto, X. Vidal, and G. Molina-Terriza, Nat. Commun. **5**, 4922 (2014).

[28] X. Zambrana-Puyalto, X. Vidal, I. Fernandez-Corbaton, and G. Molina-Terriza, Sci. Rep. **6**, 22185 (2016).

[29] M. Revah, S. Nechayev, and Y. Gorodetski, Opt. Lett. **43**, 4374 (2018).

[30] I. Fernandez-Corbaton, Helicity and duality symmetry in light matter interactions: Theory and applications, Ph.D. thesis, Macquarie University, 2014.

[31] I. Fernandez-Corbaton and C. Rockstuhl, Phys. Rev. A **95**, 053829 (2017).

[32] I. Fernandez-Corbaton, J. Phys. Commun. **2**, 095002 (2018).

[33] L. Novotny and B. Hecht, *Principles of Nano-Optics* (Cambridge University Press, Cambridge, 2012).

[34] Mirror reflections preserve purely TE polarized beams ($\psi = \pm 90^\circ$) up to a constant phase of π, rendering them achiral.

[35] M. Neugebauer, S. Nechayev, M. Vorndran, G. Leuchs, and P. Banzer, Nano Lett. **19**, 422 (2019).

[36] S. Nechayev, J. S. Eismann, M. Neugebauer, P. Woźniak, A. Bag, G. Leuchs, and P. Banzer, Phys. Rev. A **99**, 041801(R) (2019).

[37] k_{eff} depends on the focusing system [33] and is limited by the wave number: $0 \leqslant k_{\text{eff}} \leqslant k_0$. In paraxial approximation, $k_{\text{eff}} \approx k_0$; the proportionality constant A can be chosen real without the loss of generality and it can be calculated using Debye intergal [33].

[38] Craig F. Bohren and Donald R. Huffman, *Absorption and Scattering of Light by Small Particles* (John Wiley & Sons, New York, 1983).

[39] P. Woźniak, P. Banzer, and G. Leuchs, Laser Photonics Rev. **9**, 231 (2015).

[40] S. Nechayev, M. Neugebauer, M. Vorndran, G. Leuchs, and P. Banzer, Phys. Rev. Lett. **121**, 243903 (2018).

[41] P. Gutsche and M. Nieto-Vesperinas, Sci. Rep. **8**, 9416 (2018).

[42] X. Zambrana-Puyalto and N. Bonod, Nanoscale **8**, 10441 (2016).

[43] Extinction of helicity from an incident field upon interaction with a dipolar particle (right-hand side of Eq. (28) in Ref. [15]) is written in the helicity basis representation as a sum of functions of dipole polarizabilities, which are multiplied by either helicity density, energy density, or an interference term $\propto \Im\{\mathbf{E}^- \cdot \mathbf{E}^{+*}\}$ of three-dimensional RCP ($\mathbf{E}^-$) and LCP ($\mathbf{E}^+$) components of the excitation field [16,20]. This interference term can be nonzero even if the incident field has zero helicity and zero helicity density [20], as in the case of a focused SPCVB. *Conversion* of helicity is proportional to this interference term, as appears in Eqs. (3.6) and (9) in Refs. [20] and [16], respectively, and it is discussed in great detail in Refs. [16,20,41].

[44] P. Banzer, U. Peschel, S. Quabis, and G. Leuchs, Opt. Express **18**, 10905 (2010).

[45] L. Marrucci, C. Manzo, and D. Paparo, Phys. Rev. Lett. **96**, 163905 (2006).

[46] E. Karimi, G. Zito, B. Piccirillo, L. Marrucci, and E. Santamato, Opt. Lett. **32**, 3053 (2007).

[47] P. B. Johnson and R. W. Christy, Phys. Rev. B **6**, 4370 (1972).

[48] M. W. Knight, Y. Wu, J. B. Lassiter, P. Nordlander, and N. J. Halas, Nano Lett. **9**, 2188 (2009).

[49] A. E. Miroshnichenko, A. B. Evlyukhin, Y. S. Kivshar, and B. N. Chichkov, ACS Photonics **2**, 1423 (2015).

[50] K. Y. Bliokh, J. Dressel, and F. Nori, New J. Phys. **16**, 093037 (2014).

[51] L. Novotny, M. R. Beversluis, K. S. Youngworth, and T. G. Brown, Phys. Rev. Lett. **86**, 5251 (2001).

[52] O. G. Rodríguez-Herrera, D. Lara, K. Y. Bliokh, E. A. Ostrovskaya, and C. Dainty, Phys. Rev. Lett. **104**, 253601 (2010).

[53] P. Banzer, M. Neugebauer, A. Aiello, C. Marquardt, N. Lindlein, T. Bauer, and G. Leuchs, J. Eur. Opt. Soc. **8**, 13032 (2013).

[54] A. Aiello, P. Banzer, M. Neugebauer, and G. Leuchs, Nat. Photonics **9**, 789 (2015).

[55] G. F. Quinteiro, F. Schmidt-Kaler, and C. T. Schmiegelow, Phys. Rev. Lett. **119**, 253203 (2017).

[56] D. Rajesh, S. Nechayev, D. Cheskis, S. Sternklar, and Y. Gorodetski, Appl. Phys. Lett. **113**, 261104 (2018).

[57] P. Woźniak, I. De León, K. Höflich, G. Leuchs, and P. Banzer, arXiv:1902.01731.

[58] S. Nechayev, J. S. Eismann, G. Leuchs, and P. Banzer, Phys. Rev. B **99**, 075155 (2019).